Assessment of Environmental Parameters in Natural Coastal Scenery and Compositional by Means of an Innovative Approach

atmosphere

MDPI

Article

Assessment of Environmental Parameters in Natural Coastal Scenery and Compositional by Means of an Innovative Approach

Nicole Mastromatteo *, Lia Drudi, Davide Gallione, Rossana Bellopede and Marina Clerico

Department of Environmental, Land and Infrastructure Engineering (DIATI), Polytechnic University of Turin, 10129 Turin, Italy; lia.drudi@polito.it (L.D.); davide.gallione@polito.it (D.G.); rossana.bellopede@polito.it (R.B.); marina.clerico@polito.it (M.C.)

* Correspondence: nicole.mastromatteo@polito.it

Abstract: Three measurement campaigns were conducted on the island of Culuccia (Sardinia, Italy) to evaluate particulate matter (PM) concentrations and the contribution of sea spray aerosol (SSA) across different seasons in a largely uncontaminated coastal environment. The goal is not only to analyze PM concentration in relation to meteorological parameters such as temperature, relative humidity (rH), and wind speed but also to provide a chemical analysis of SSA. The chemical composition of PM was determined using Raman spectroscopy and SEM-EDX, allowing for precise identification of individual particles. Results showed seasonal variations in PM composition, with sodium nitrate and sodium chloride prevalent in March and June and sulfates dominating in October. A correlation between the PM composition and meteorological parameters was observed according to the value of the deliquescence relative humidity (DRH), highlighting the reciprocal influence of rH and coarse and fine PM trends. This multi-technique approach offers valuable insights into the relative abundance of different PM compound classes based on the varying conditions for SSA formation. This enhances our understanding of the behavior of sea spray aerosol and other PM in natural coastal environments.

Keywords: sea spray aerosol; atmospheric chemistry; PM concentration trend; meteorological parameter; PM chemical composition; Raman spectroscopy; SEM-EDX

Citation: Mastromatteo, N.; Drudi, L.; Gallione, D.; Bellopede, R.; Clerico, M. Assessment of Environmental Parameters in Natural Coastal Scenery and Compositional by Means of an Innovative Approach. *Atmosphere* **2024**, *15*, 1379. https://doi.org/10.3390/atmos15111379

Academic Editors: Bin Chen, Ning Tang and Bushra Khalid

Received: 10 October 2024
Revised: 24 October 2024
Accepted: 2 November 2024
Published: 15 November 2024

1. Introduction

Aerosol particles in the atmosphere can originate from a variety of natural processes, including wind-borne dust, sea spray, volcanic debris, biogenic aerosol, and biological material [1]. Among these, sea spray droplets are the most numerous in terms of mass [1]. Marine aerosol is a complex mixture of sea salt, organic material, and water, with major constituents including organic matter, sodium, calcium, magnesium, potassium, chlorine, and sulfates [2,3]. Sea spray aerosol (SSA), together with mineral dust, emerges as one of the primary aerosols worldwide concerning the mass discharged into the atmosphere [4] and plays a major, largely undetermined role in affecting our atmosphere [5]. The contribution of SSA to atmospheric aerosol loading varies temporally and spatially, with significant implications for air quality, human health, and radiative forcing [6]. Specifically, sea spray can be formed through the breaking of sea waves [7], the bursting of bubbles, and the breaking of wave crests, resulting in the formation of white cap [8]. The formation of white caps is governed by complex physical laws influenced by various factors that are challenging to measure and monitor effectively [9]. Sea spray droplets, resulting from the bursting of bubbles, may be transported to the upper atmosphere [10] and remain in suspension for many days [11]. These particles, influenced by solar radiation, can evaporate and decrease until they lose their water content. Air bubbles collect organic matter from the surrounding seawater, and when these bubbles burst, they produce SSA that are enriched in organic matter [12]. They also carry dissolved gases, salts, and biological materials, the chemical composition of which is determined by the way they were

formed. This study aims to investigate sea spray particles due to their significance, but with an innovative approach combining PM concentration analysis with meteoclimatic parameters and quantification of the main PM components by chemical analysis. The goal is to address the challenges of monitoring the complex variables involved in white cap formation while also correlating PM concentration measurements with theoretical and observed meteorological and climatic parameters. This approach seeks to provide a more comprehensive understanding of physical phenomenon. This aims to bridge the limited knowledge of how SSA and other particulate matter (PM) in natural coastal environments interact with meteorological and climatic parameters, particularly in scenarios with minimal anthropogenic pollution. This highlights the gap in current PM monitoring and analysis techniques in coastal regions. A comprehensive examination of the existing literature reveals a consistent trend: an escalation in relative humidity correlates with a decrease in the concentrations of fine aerosol particles. Understanding the impact of relative humidity (rH) on particulate matter (PM) concentration is paramount, given the variability introduced by sedimentation processes [13]. Atmospheric moisture increases the mass of smaller particles, promoting their sedimentation. Exploration of PM deposition at various humidity levels becomes imperative, considering that the hygroscopicity and growth rate of PM are contingent on factors such as composition, size, ambient temperature, and humidity [14,15]. Noteworthy precursors, including sulfate (SOx), nitrate (NOx), ammonium (NH_3), volatile organic chemicals, and reaction intermediates, significantly contribute to the atmospheric concentration of PM2.5 [13]. Ultimately, a single-particle characterization is carried out employing a combination of two distinctive techniques: Raman spectroscopy (RS) and Scanning Electron Microscope with Energy-Dispersive X-ray (SEM-EDX). Raman Microspectroscopy can identify the chemical composition of typical aerosol particles by their characteristic peak [16], preventing any sample preparation. This technique can provide an unambiguous identification of the different PM chemical species correlating their characteristic vibrational modes to the resulting Raman spectra [17]. Additionally, it is a non-destructive, non-invasive, and repeatable technique [18]. Unfortunately, it cannot detect some components such as NaCl [19], one of the most present salts in sea spray aerosol, due to its ionic structure [20]. Instead, SEM analysis can provide critical information about the morphology associated with the formation and transportation process of a single PM particle. The shape of the particle car varies greatly: from flocculent and spherical shape to regular crystalline and irregular shape [21]. Furthermore, using SEM with an EDX detector has demonstrated its suitability for analyzing the elemental composition of individual solid dry particles with submicron lateral resolution. Automated SEM-EDX can provide quantitative information on the elemental composition of a large number of particles and has been used successfully to characterize a range of atmospheric aerosol samples [22]. The combined application of Raman spectroscopy and Scanning Electron Microscopy with Energy-Dispersive X-ray analysis for investigating the composition of particulate matter has been established in numerous studies [20,22–27]. The innovation in this study is to consider these two techniques on the same particle, as opposed to what is usually performed when using this combined application. Our powerful approach offers a comprehensive understanding of PM by simultaneously revealing its molecular composition and structure, elemental composition, size, and morphology. Critically, employing both techniques on the same particle significantly enhances identification accuracy through mutual confirmation and expanded detection range. This comprehensive approach has proven valuable in previous research but, in this work, provides a new and unique method by quantifying the proportions of different PM compounds across the three different time periods considered, allowing a comparative analysis of the principal PM components. This single-particle analysis enables a more nuanced understanding of the factors influencing PM composition and its potential health and environmental impacts. Furthermore, this study was able to establish correlations between compositional analysis, meteorological parameters, and trends in PM2.5 levels, providing valuable insights into the factors driving PM formation and transport in the studied region.

2. Materials and Methods

2.1. Site and Sampling Description

The measurement operations were carried out on Culuccia island, a peninsula of 300 hectares on the northeast coast of Sardinia, located between Porto Pollo and Porto Pozzo, in the province of Sassari (Figure 1). Before this research, no air quality measurement campaigns had ever been carried out on Culuccia island by other researchers. The present study consisted of three different campaigns. The first measurement campaign lasted from 11 March to 18 March 2023. The second campaign lasted from 21 June to 28 June 2023, and the last from 30 September 2023 to 12 October 2023. The decision to repeat the measurement campaigns at different times of the year was made to best consider the measurement of PM concentrations with different boundary conditions and to understand what changes in the different seasons should be considered. A preliminary campaign was made from 16 November to 24 November 2022. For this campaign only, the analyses did not include chemical analyses because, due to adverse weather conditions, the collected samples were not appropriate for RS and SEM-EDX analysis. Therefore, in Graph S1 in the Supplementary Materials, the trends of different PM fractions monitored during this campaign are reported. For each campaign, data were collected from Palas Fidas 200S for the various particle size fractions (PM1, PM2.5, PM4, PM10) as a function of time. In all campaigns, the Palas Fidas 200S was placed in a location that best represents the weather conditions of the area (41.203099 N, 9.290897 E). Remarkably, this island has been home to a lone inhabitant for over 73 years. The unique landscape of Culuccia island is safeguarded by various regulations addressing diverse environmental aspects. This protection reflects the commitment to preserving the island's rich biodiversity and ensuring the sustainable coexistence of its ecosystems. Hence, the choice of the island as a pollutant-free location in which to carry out measurements allowed us to capture PM concentrations without the intervention of dust from anthropogenic sources.

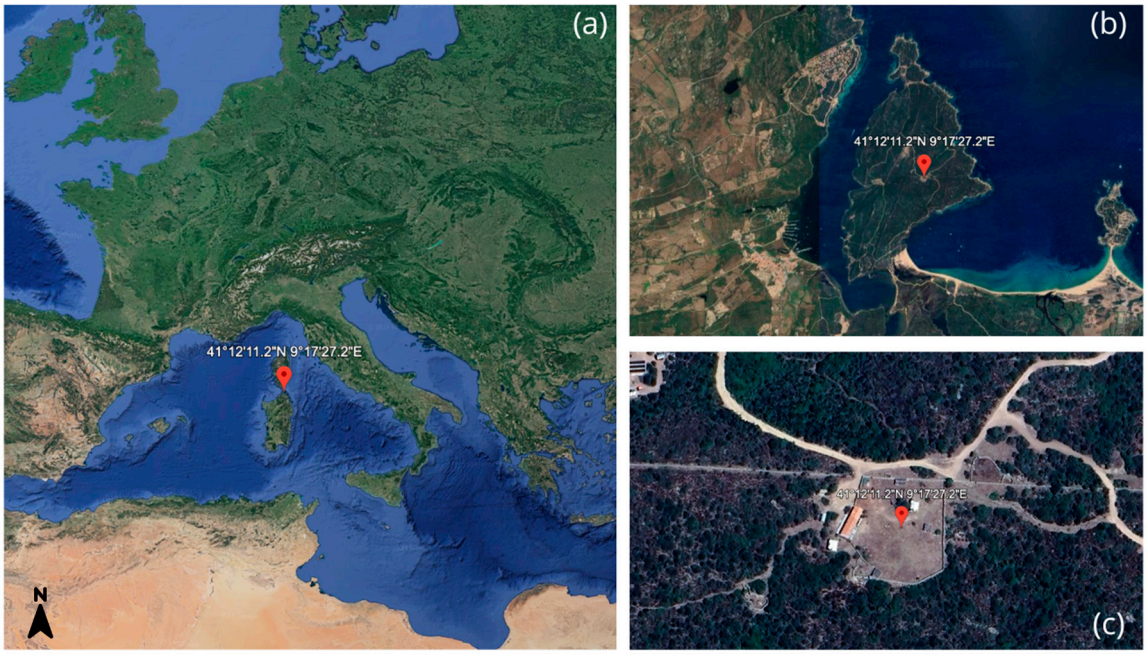

Figure 1. Aerial image of Culuccia island (source: Google Earth). Visualization of overall Italy (**a**), Culuccia island specifically (**b**), and the exact location (**c**) of the Palas Fidas 200S during the measurement campaigns.

2.2. Palas Fidas 200S

The Palas Fidas 200S analyzer is an instrument that can measure the concentration of solid particles ranging in size from 180 nm to 18 microns. The parameters acquired are

PM1, PM2.5, PM4, PM10, and PTS. The external configuration of the instrument includes a stainless-steel container to protect it from the weather and keep the instrument at an optimal temperature for measurements. The instrument is equipped with a sensor and an optical spectrometer that allows the definition of the number of aerosol particles and their size, thanks to the scattering phenomenon. Each particle will produce a light pulse picked up by the sensor; the number of pulses recorded will be directly related to the number of particles, while the intensity of the pulses will be associated with the diameter of the same. The acquired signal will return the number of particles and their size distribution. The sampling head can capture a flow of 0.3 m^3/h and enables representative measurements even in intense wind, thanks to the Sigma-2 sampling head with VDI 2119-4. The instrument is equipped with an IADS (Intelligent Aerosol Drying System), from Palas GmbH Germany, as well as sensors for measuring the temperature, air pressure, and relative humidity. The IADS prevents incorrect measurements caused by condensation effects in areas with high humidity. The temperature must be kept higher than the dew temperature, which is why a mechanism inside the drying line regulates it according to the external temperature, pressure, and rH. During the measurement campaigns, Polytetrafluoroethylene (PTFE) filters were kept inside the Palas Fidas 200S for the entire duration of each campaign to collect PM particles.

2.3. Raman Spectroscopy

For the micro-Raman analyses, an inVia Raman confocal spectrophotometer coupled to a LEICA microscope was utilized. For each of the collected filters, PM particles with a geometric size between 1 and 10 μm were randomly selected in five distinct areas and then analyzed. Specifically, a reference system was implemented for each filter, and the coordinates of each particle along the five areas were saved to facilitate the relocation of the particles in subsequent SEM-EDX analyses. No pretreatment was required for the samples before analysis. The measurements were performed employing a 532 nm Diode Pumped Solid State (DPSS) laser, set to a power of 250 μW (nominal power of 50 mW) to avoid sample thermo-decomposition. The Raman spectrophotometer was properly calibrated using the 520.7 cm^{-1} peak of a silicon wafer. The acquisition time was 15 s, and each spectrum was integrated over four accumulations to improve the Signal-to-Noise Ratio (SNR). The Wire 5.6 software package (Renishaw) was used to perform the data acquisition, and the acquired Raman spectra were interpreted by consulting the Renishaw built-in database. Furthermore, free Raman databases (e.g., RRUFF) were equally considered for assigning Raman bands [28]. For each acquired Raman spectrum, post-processing consists of smoothing and baseline removal. The smoothing is performed by implementing the Savitzky–Golay algorithm to improve the SNR.

2.4. SEM-EDX

After the Raman measurement, the PM samples were coated with a 5 nm thin layer of gold film using a QUORUM Q150R S sputter coater (QUORUM, Judges House, Lewes Road, Laughton, East Sussex., UNITED KINGDOM). The measurements were carried out using a QUANTA INSPECT 200LV microscope (FEI COMPANY, Hillsboro, OR, USA) coupled with an EDX detector (EDAX (Ametek Inc.), Mahwah, NJ, USA). Using the coordinates selected before, it was possible to relocate the same areas and analyze each particle that had been previously examined by Raman spectroscopy (Renishaw S.p.A. Wotton-under-Edge, UK). SEM images were obtained for the same five areas, and EDX spectra were collected for the selected particles in order to further characterize their elemental composition.

3. Results

3.1. Temporal and Spatial Analysis of Particulate Matter

In the preliminary studies conducted based on an initial measurement campaign that took place from 16 November 2022 to 24 November 2022, it was important to observe the Pearson correlation indices between various particulate fractions and various meteoclimatic

parameters. Table S1 in the Supplementary Materials shows the Pearson correlation indices of the main parameters measured during the preliminary campaign on Culuccia island. It follows from this first study that in uncontaminated scenarios, there is also a high correlation between PM generation and wind speed. Wind speed was measured with a Davis Vantage Pro 2 weather station. Higher wind speed corresponds to an increase in the generation of the various PM fractions. Considering the significant influence that all meteoclimatic parameters exert on PM concentrations, such as temperature [29], wind speed, relative humidity, solar radiation, etc., in this study, it was preferred to include and give greater importance to the significant correlation these parameters have with relative humidity regarding the compositional analysis of the particles. Precipitation was not considered since rainfall events were too few in all three measurement campaigns. In the Supplementary Materials, there is an explanation of the weather and climate conditions in the area. Although all PM particle size fractions were scientifically measured, it was voluntarily preferred to present the results for PM2.5, as it was more representative of the specific scenario analyzed and the considerable size of the apparent prevalence of particles collected on the filter.

Figure 2 shows the results of the three measurement campaigns in terms of concentration of PM2.5 and relative humidity over time. During the first campaign, in March, the weather–climate conditions are representative of a winter season, with temperatures averaging 13.34 °C and an average rH of 72.65%. The average value of PM2.5 is 6.55 μg/m^3, while that of PM10 is 11.90 μg/m^3. Table S1 in the Supplementary Materials shows the average values of all PM fractions together with the average values of relative humidity and temperature, measured in all three campaigns (March, June, and October). In this campaign, there are less-pronounced day–night alternation rH trends due to the particular weather and climate conditions on the island at that time. The second campaign (Figure 2), conducted in June, shows average temperatures of 25.27 °C and an average rH of 71.99%. Evident from the graph is the typical trend of relative humidity following the day–night alternation. The average value of PM2.5 is 10.39 μg/m^3, while that of PM10 is 22.76 μg/m^3. This campaign recorded the highest concentration values in terms of atmospheric particulate matter; this may be due to the increased anthropogenic activity, mainly tourism and island management. The last campaign, which is the longest in duration, was conducted between September and October, with average temperatures of 22.34 °C and an average rH of 77.06%. Also evident from the graph is the typical trend of relative humidity because of the day–night alternation: the highest values of rH are recorded during the day, which correspond to the lowest values recorded for PM. The average value of PM2.5 is 7.25 μg/m^3, while that of PM10 is 12.02 μg/m^3. On average, the PM2.5/PM10 ratio is around 0.5: 0.55 for the March campaign, 0.46 for the June campaign, and 0.60 for the October campaign. These ratios confirm the presence of dust of natural origin, which typically occupies the coarsest fraction of the particle size curve.

3.2. Identification of the Chemical Composition

Particles deposited on the filter have a broad range of shapes and sizes (Figure 3). PM morphology heterogeneity is heavily correlated to the diverse structures, origin, and composition of these particles. The varied morphology of the particles suggests the presence of different sources and formation processes, contributing to the intricate nature of marine aerosol particles. In the Supplementary Materials, a brief explanation of the main formations and significance of secondary inorganic salts is provided.

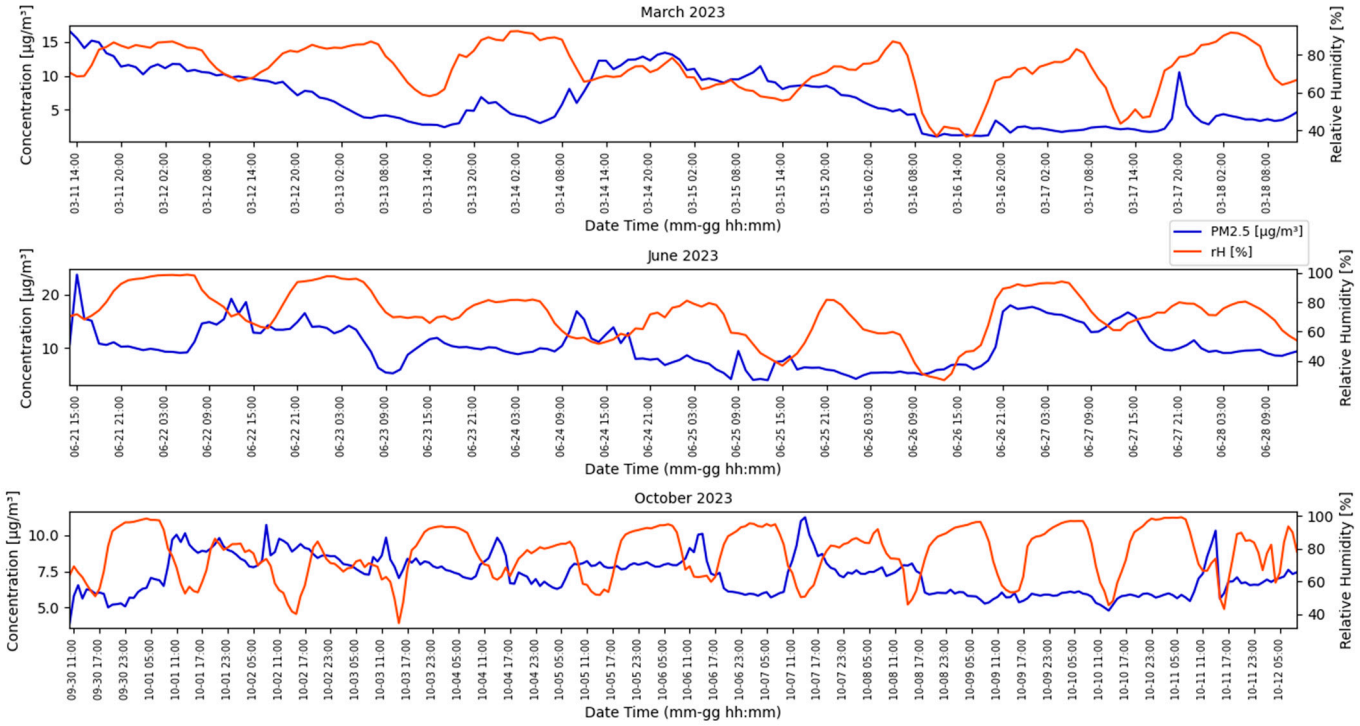

Figure 2. PM2.5 concentration trend (in blue) and rH (%) trend (in red) in the three measurement campaigns (March, June, and October).

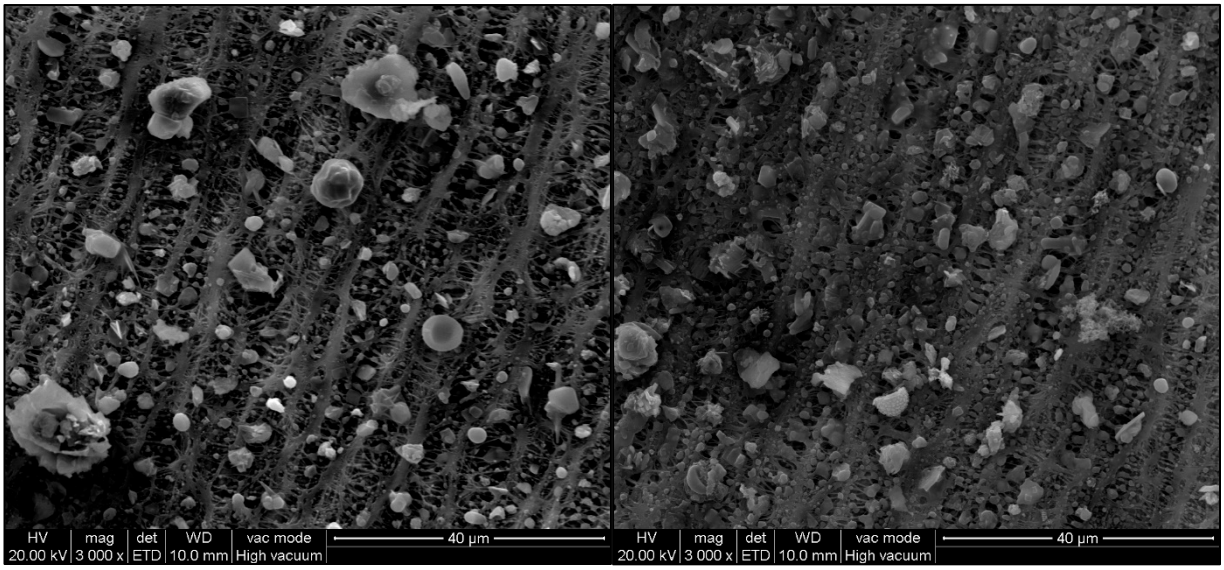

Figure 3. SEM images of PM particles from the June (**left**) and October (**right**) campaigns.

About 70 particles, carefully collected during each sampling campaign, were thoroughly analyzed, and Raman and EDX spectra were collected for each particle. The EDX spectra may be affected by the composition of the PTFE filter, which displays peaks for C and F. Additionally, interference can occur from the nanometric layer of gold through the Au-peak. Although carbon remains useful for identifying compounds, Figure 4 reports the F and Au peaks in red. The Raman spectra can be influenced by fluorescence, which can interfere with the identification of compounds. To reduce this effect, a lower laser power was employed. Eight different classes were selected to analyze the composition of the fine and coarse PM: carbon material, silicon-rich particles, sodium chloride, sulfate salts, nitrate salts, calcite, iron, and titanium oxide. If the analysis identified multiple classes, the particle

was regarded as a cluster comprised of individual compounds considered separately in this study. Raman and SEM spectra of four distinct particles, representative of the primary class under investigation in this study, were selected from the June expedition for analysis (Figure 4).

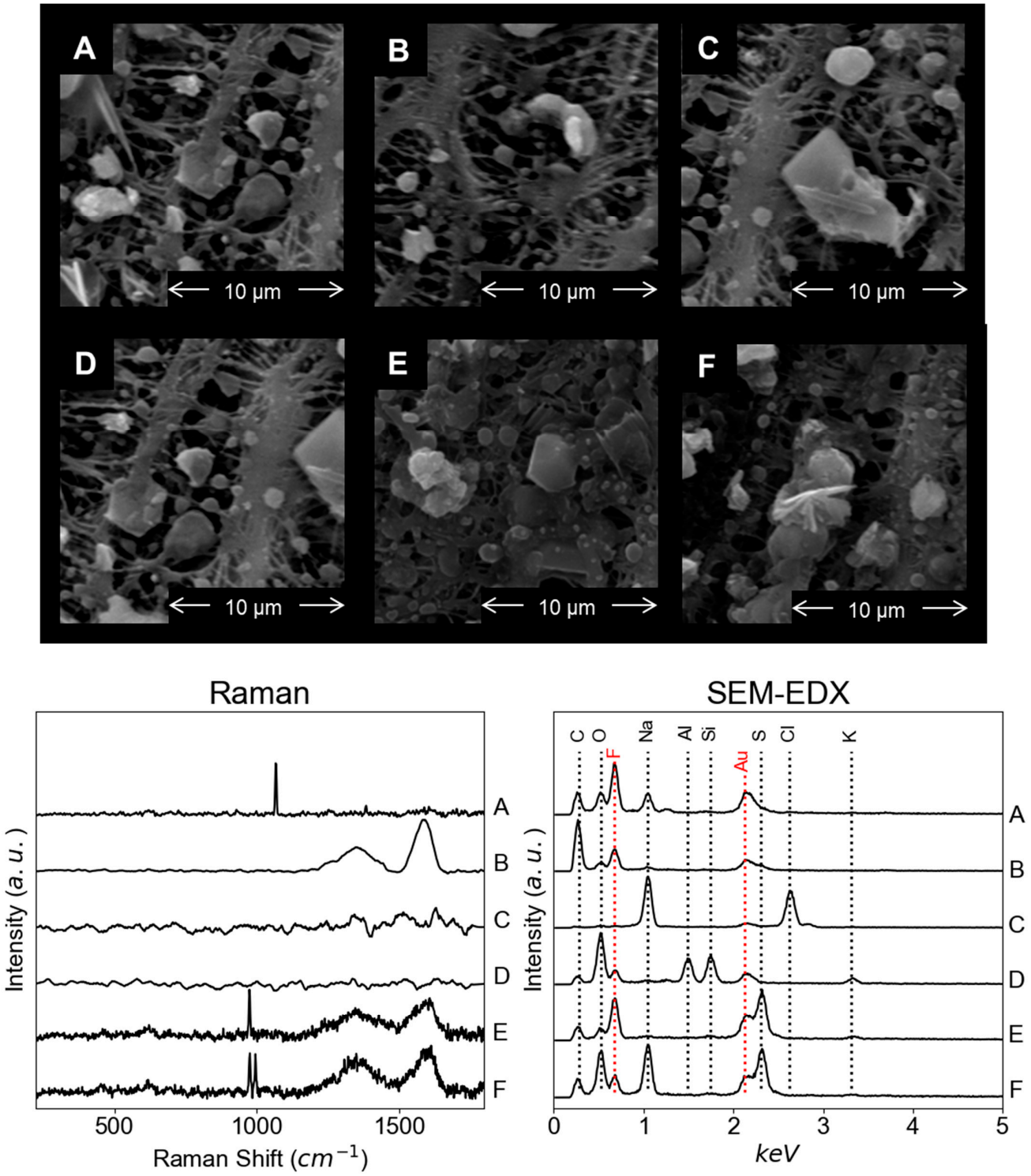

Figure 4. SEM images (**first subfigure**) of main components observed in the different sampling analyses: (**A**) sodium nitrate, (**B**) carbon, (**C**) sodium chloride, (**D**) silicon-rich, (**E**) ammonium sulfate, (**F**) ammonium and sodium sulfate and their relative Raman spectra (**left**) and EDX spectra (**right**).

In this study, nitrate salts, primarily composed of sodium nitrate, are mainly present during the March and June campaigns, while sulfate salts dominate the October campaign. Nitrate salts are more effortlessly recognized with Raman spectroscopy because the N-peak in the EDX spectra cannot always be visible from interference from C, O, and the Bremsstrahlung background [30]. Hence, the particle is assigned to the nitrate class if the EDX spectra confirm the presence of the expected cation. Figure 4, spectrum A shows an example of the identification of sodium nitrate, with a prominent peak at 1067 cm^{-1} Raman shift and the Na-peak in the EDX spectra. In addition to sodium nitrate, a negligible amount of calcium and ammonium nitrate was found. Ammonium nitrate can be particularly challenging to detect using SEM-EDX spectra because of interferences. However, it is identifiable through Raman spectroscopy [31,32]. The morphology of nitrate salts in PM is complex and influenced by a range of factors [33]. In this study, they usually exhibit a regular shape (Figures 3 and 4).

The Raman spectrum of carbon typically features prominent peaks at approximately 1580 and 1350 cm^{-1}, as shown in Figure 4, spectrum B4. Carbon particles, especially those coming from combustion, can encase other particles, and the carbon Raman signal can sometimes obscure other peaks [34]. Hence, the particle is assigned as carbon only if the EDX measurement also shows a strong C-peak. Alternatively, if the EDX measurement indicates elements other than carbon, it is considered the other class. Carbon particles in PM can exhibit a range of morphologies, including spherical, agglomerated, and agglomerated with organic material [35–37]. In this study, the agglomerated form is frequently observed (Figures 3 and 4). In addition, a small amount of pollen was found and identified because of the characteristic peaks of pollen [38–40], the prominent C-peak in the EDX measurement, and the morphology of the particles.

Sodium chloride cannot be detected by Raman spectroscopy due to its ionic bonds [20], so the identification is possible only with SEM-EDX measurements through the Cl and Na peaks [32]. In Figure 4, spectrum C, the Raman result shows no relevant peaks, while the EDX spectra show the Na-peak and the Cl-peak. The shape of sodium chloride in PM can vary based on environmental conditions, such as temperature, moisture, and other factors. It can exist as clusters or individual particles, and sometimes it forms larger agglomerates due to various influences [41]. Sodium chloride typically displays a structured pattern in SEM images and is commonly found clustered with other particles (Figures 3 and 4).

From the acquired Raman spectra, it can be inferred that only a restricted set of particles has displayed peaks, suggesting the existence of crustal particles. Conversely, in EDX analysis, when the same particle exhibits a significant amount of Si, as well as other crustal elements such as Al, Mg, Ca, and K, for this classification, the particle is considered a crustal particle only if the Si-peak in the EDX spectra is dominant and there are other elements typical of a crustal particle (Figure 4, spectrum D). The morphology of the particles is often irregular and varied, exhibiting diverse shapes and sizes (Figures 3 and 4). The October campaign indicates a considerable amount of sulfate in both forms of ammonium sulfate and sodium sulfate, often together (Figure 4, spectra E and F). For ammonium sulfate, the main peak occurs at a Raman shift of 975 cm^{-1} [17], while for sodium sulfate, it appears at 994 cm^{-1} (Figure 4). Alternatively, The SEM-EDX measurement confirms the presence of the S-peak in both cases and the presence of Na for sodium sulfate, while the N-peak is not observed due to interference (Figure 4, spectra E and F). Hence, the identification is easier with Raman spectroscopy. Moreover, the S-peak is present in a considerable number of other particles, which indicates an intense amount of sulfate salt deposited on other particles. Practically negligible amounts of calcite are present in all three samples. This can be detected by the main peak at 1018 cm^{-1} Raman shift (R150020 of RRUFF database) and by the presence of C and Ca in the SEM-EDX spectra. Different Raman spectra have been identified as iron oxide. One spectrum from the March campaign shows a broad band with a peak at 662 cm^{-1} Raman Shift, which is consistent with magnetite RRUFF (R080025 with 532 nm), while one Raman spectrum from the June campaign shows different bands, which are consistent with hematite (R050300). The EDX analysis confirms the presence of

iron in both cases. In the October campaign, one spectrum shows titanium oxide in the form of anatase with a main peak at 144 cm^{-1} (R070582), and the corresponding SEM-EDX spectra show the Ti-peak. Both compounds have already been found in previous studies on PM [17,42,43].

3.3. Composition Analysis of Particulate Matter

In Figure 5, we observe the main components found in the three different samplings of March, June, and October. The reported percentages indicate categorization based on the quantity of coarse and fine particles analyzed. The primary compounds include carbon, silicon material, and salts like nitrate, sulfate, and sodium chloride. Other classes like calcite, iron oxide, and titanium oxide are not present in significant amounts and, hence, are not crucial for this analysis.

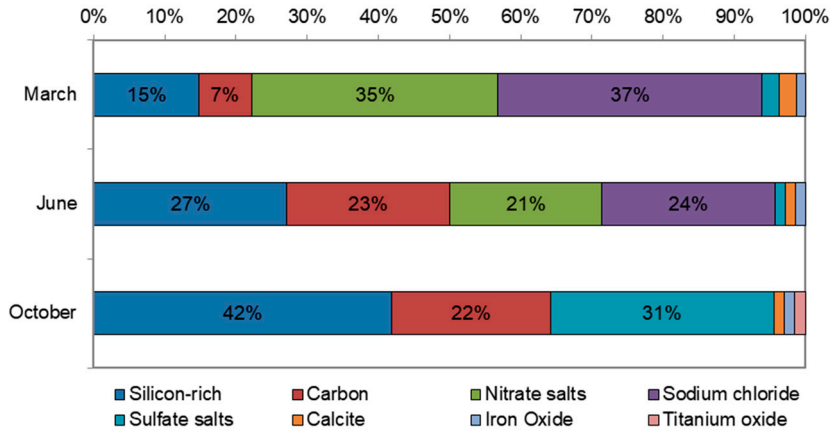

Figure 5. The proportion of identified PM components.

Silicon-rich and carbon particles are present in all three campaigns in considerable amounts with different percentages. The carbon content is lower in the March campaign and higher in the June campaign, reaching 42% of the total analyzed particles in the October campaign. Additionally, for the silicate class, a lower amount was found in the March campaign, while an almost identical percentage of 23% was determined in the other two campaigns.

The mean levels of PM10 and PM2.5 in the March and October campaigns are close, but they are nearly twice as high in the June campaign. When analyzing the PM10 trend in October, very prominent peaks can be found on the following dates: 2 October 2023 at 8:00 am and 11 October 2023 at 2:00 pm. These are the results of constructional operations in the surrounding area of sampling, contributing to a significant increase in silicate and carbon levels due to PM production and resuspension. During both the March and June campaigns, a significant quantity of sodium chloride and nitrate salts (predominantly sodium nitrate) was detected. The proportions were similar in both groups during each campaign, with a higher level observed during the March campaign, although we should take into account the lower average amount of PM discovered. In the October campaign, there is a considerable amount of sulfate salts. According to the Raman result, two main salts were found: ammonium sulfate and sodium sulfate. A total of 45% of the particles analyzed correspond to sodium nitrate, while ammonium sulfate corresponds to 55%.

Deliquescence is a property exhibited by certain substances, typically salts, wherein they display a pronounced affinity for atmospheric moisture. Consequently, these compounds absorb water and tend to dissolve, generating a solution until a state of equilibrium is achieved between the vapor pressure on the aqueous solution and the partial pressure of water in the surrounding atmosphere. When the relative humidity surpasses a specific threshold known as the deliquescence point, a crystalline particle of saline aerosols undergoes deliquescence in the atmosphere. Examples of universal deliquescent substances

include salts like calcium chloride, magnesium chloride, zinc chloride, and sodium carbonate. The value of deliquescence relative humidity (DRH), therefore, represents the point of atmospheric relative humidity above which the salt absorbs water to form a saturated aqueous solution. When the atmospheric rH takes values below DRH, the salt remains in the solid phase. Beyond DRH, if the rH continues increasing, additional and more water condenses on the particle to maintain thermodynamic equilibrium. For example, nitrate production can be enhanced when the relative humidity is higher than the deliquescence point of ammonium nitrate [44]. When analyzing marine spray particles, it is important to consider their composition and mixing state to model their hygroscopic behavior and subsequent atmospheric impacts. Environmental marine aerosol particles showed multiple deliquescence and efflorescence transitions, mainly influenced by NaCl, $NaNO_3$, $MgCl_2$, $Mg(NO_3)_2$, and organic species covering the surface of elderly ones. In addition, the aged mineral particles showed partial or complete phase changes with varying relative humidity due to the presence of nitrate species [45]. To clarify the distribution of diverse compound classes, we compared the average rH values documented throughout the entire campaign with the DRH values commonly linked to the specific classes of compounds under investigation. The compounds analyzed were $NaNO_3$, NH_4NO_3, NaCl, Na_2SO_4, and $(NH_4)_2SO_4$, with deliquescence values of 74.5%, 61.83%, 75.28%, 84.2%, and 79.97%, respectively [46]. These compounds were taken as a reference because ammonia, sulfate, nitrate, sodium, and chloride are the dominant components of reactive inorganic aerosols in the atmosphere [47]. Table 1 confirms the results in Figure 5. $NaNO_3$ was found only during the March (35%) and June (21%) campaigns, as the rH% was below the DRH value (74.5%). NH_4NO_3 was never detected because the average rH% recorded was higher than the DRH value. Particulate ammonium nitrate typically forms under conditions of low temperatures and relative humidity that exceed its deliquescence point [44]. NaCl is present in higher percentages, 37% and 24%, in the first two campaigns, respectively, and absent in the last campaign (October). It should be kept in mind that it evaluates NaCl in crystal form and, therefore, in solid phase and not in aqueous form. In that case, that component would be lost in the heating of IADS, which has the function of removing water vapor from the particle before measurement. Sulfate salts, on the other hand, are present in different percentages in all three measurement campaigns because the measured rH value is lower than the DRH (%).

Table 1. Table correlating the DRH value (%) of the main salts found in the literature with the relative humidity value (rH %) measured in the three campaigns. Green cell color indicates corresponding rH(%) < DRH (%), while red cell color indicates rH(%) > DRH.

Chemical Compound	DRH (%)	rH(%) Average Value Measured		
		March	June	October
$NaNO_3$	74.5	72.65	72.00	77.06
NH_4NO_3	61.83	72.65	72.00	77.06
NaCl	75.2	72.65	72.00	77.06
Na_2SO_4	84.2	72.65	72.00	77.06
$(NH_4)_2SO_4$	79.97	72.65	72.00	77.06

4. Conclusions

The analysis of PM collected during the campaigns provided valuable insights into the composition of atmospheric aerosols. The identification of various compounds such as nitrate salts, sulfate salts, carbon, sodium chloride, and crustal particles was effectively carried out using an innovative and multimodal approach by Raman and SEM-EDX spectroscopy. Notably, the presence of nitrate salts, primarily composed of sodium nitrate, was prominent during the March and June campaigns, while the October campaign exhibited a significant amount of sulfate salts, including both ammonium sulfate and sodium sulfate. The detection of these compounds was made possible through the distinctive peaks observed in the Raman spectra, along with confirmation from SEM-EDX measurements.

The phenomenon of deliquescence, characterized by the strong affinity of certain substances, especially salts, for atmospheric moisture, plays a significant role in atmospheric processes. The absorption of water by these compounds, resulting in the formation of saturated aqueous solutions, is governed by the equilibrium between the vapor pressure on the solution and the partial pressure of water in the surrounding atmosphere. The innovative approach is highlighted by the fact that PM fractions were correlated with the rH parameter. The latter has been linked to the deliquescence relative humidity (DRH). This has allowed us to explain the presence of different types of secondary salts found through compositional analysis. Indeed, the deliquescence point, a specific threshold in relative humidity, initiates the transition of crystalline particles of saline aerosols into a solution in the atmosphere. In this investigation, comparing average relative humidity values with the DRH values for specific compound classes such as $NaNO_3$, NH_4NO_3, NaCl, Na_2SO_4, and $(NH_4)_2SO_4$ yielded valuable insights. This analysis sheds light on the interaction of these compounds with atmospheric moisture and their undergoing deliquescence across diverse environmental conditions. Consequently, it enhances our understanding of atmospheric processes involving various compound classes on a broader scale. The correlation between PM trend, meteorological parameters, and compositional and chemical analysis by Raman spectroscopy and SEM-EDX provided a more comprehensive and insightful understanding of atmospheric aerosols. This innovative interdisciplinary approach will not only enhance the interpretation of the obtained data but also contribute to a deeper understanding of the complex interactions and processes governing atmospheric PM.

Supplementary Materials: The following supporting information can be downloaded at: https://www.mdpi.com/article/10.3390/atmos15111379/s1. Figure S1: Pearson's correlation index for all variables measured during the first measurement campaign (preliminary campaign) held in Culuccia island from 16 November 2022 to 24 November 2022; Graph S1: Trends of different PM concentrations during the preliminary campaign on Culuccia Is-land from 16 November 2022 to 24 November 2022; Table S1: Mean values of all PM fractions measured, and mean values of relative humidity and temperature recorded in all three campaigns (March, June, and October); Graph S2: Temperature (°C) and relative humidity (rH %) trends for the March campaign; Graph S3: Temperature (°C) and relative humidity (rH %) trends for the June campaign; Graph S4: Temperature (°C) and relative humidity (rH %) trends for the October campaign.

Author Contributions: Conceptualization, N.M. and L.D.; Methodology, N.M., L.D. and D.G.; Validation, D.G.; Investigation, N.M. and L.D.; Resources, R.B. and M.C.; Data curation, N.M., L.D. and D.G.; Writing—original draft, N.M. and L.D.; Writing—review & editing, N.M. and L.D.; Supervision, R.B. and M.C.; Project administration, R.B. and M.C. All authors have read and agreed to the published version of the manuscript.

Funding: There is no funding for this manuscript. Our grant will be used to cover APCs.

Institutional Review Board Statement: Not applicable.

Informed Consent Statement: Not applicable.

Data Availability Statement: All figures in the text and specific data used for this research study are available on request from Prof. Marina Clerico and Prof. Rossana Bellopede, according to policies from the Politecnico di Torino.

Acknowledgments: We gratefully acknowledge the "Osservatorio Naturalistico Isola di Culuccia" for their support and collaboration in this study. This publication is part of the project PNRR-NGEU, which received funding from MUR–DM 352/2022.

Conflicts of Interest: The author declare no conflict of interest.

References

1. Tomasi, C.; Lupi, A. Primary and Secondary Sources of Atmospheric Aerosol. In *Atmospheric Aerosols*, 1st ed.; Tomasi, C., Fuzzi, S., Kokhanovsky, A., Eds.; Wiley: Hoboken, NJ, USA, 2017; pp. 1–86. ISBN 978-3-527-33645-6.
2. Jacobson, M. *Atmospheric Pollution: History, Science, and Regulation. The Edinburgh Building, Cambridge CB2 8RU, UK—Published in the United States of America by Cambridge University Press*; Cambridge University Press: New York, NY, USA, 2002.

3. Harrison, R.M.; Pio, C.A. Size-differentiated composition of inorganic atmospheric aerosols of both marine and polluted continental origin. *Atmos. Environ. (1967)* **1983**, *17*, 1733–1738. [CrossRef]
4. De Leeuw, G.; Andreas, E.L.; Anguelova, M.D.; Fairall, C.W.; Lewis, E.R.; O'Dowd, C.; Schulz, M.; Schwartz, S.E. Production flux of sea spray aerosol. *Rev. Geophys.* **2011**, *49*, 2010RG000349. [CrossRef]
5. Cochran, R.E.; Ryder, O.S.; Grassian, V.H.; Prather, K.A. Sea Spray Aerosol: The Chemical Link between the Oceans, Atmosphere, and Climate. *Acc. Chem. Res.* **2017**, *50*, 599–604. [CrossRef]
6. O'Dowd, C.D.; De Leeuw, G. Marine aerosol production: A review of the current knowledge. *Phil. Trans. R. Soc. A.* **2007**, *365*, 1753–1774. [CrossRef]
7. Deike, L.; Reichl, B.G.; Paulot, F. A Mechanistic Sea Spray Generation Function Based on the Sea State and the Physics of Bubble Bursting. *AGU Adv.* **2022**, *3*, e2022AV000750. [CrossRef]
8. Lafon, C.; Piazzola, J.; Forget, P.; Le Calve, O.; Despiau, S. Analysis of the Variations of the Whitecap Fraction as Measured in a Coastal Zone. *Bound.-Layer Meteorol.* **2004**, *111*, 339–360. [CrossRef]
9. Stramska, M.; Petelski, T. Observations of oceanic whitecaps in the north polar waters of the Atlantic. *J. Geophys. Res.* **2003**, *108*, 2002JC001321. [CrossRef]
10. Richter, D.H.; Dempsey, A.E.; Sullivan, P.P. Turbulent Transport of Spray Droplets in the Vicinity of Moving Surface Waves. *J. Phys. Oceanogr.* **2019**, *49*, 1789–1807. [CrossRef]
11. Quinn, P.K.; Collins, D.B.; Grassian, V.H.; Prather, K.A.; Bates, T.S. Chemistry and Related Properties of Freshly Emitted Sea Spray Aerosol. *Chem. Rev.* **2015**, *115*, 4383–4399. [CrossRef]
12. Quinn, P.K.; Bates, T.S.; Schulz, K.S.; Coffman, D.J.; Frossard, A.A.; Russell, L.M.; Keene, W.C.; Kieber, D.J. Contribution of sea surface carbon pool to organic matter enrichment in sea spray aerosol. *Nat. Geosci.* **2014**, *7*, 228–232. [CrossRef]
13. Kim, M.; Jeong, S.-G.; Park, J.; Kim, S.; Lee, J.-H. Investigating the impact of relative humidity and air tightness on PM sedimentation and concentration reduction. *Build. Environ.* **2023**, *241*, 110270. [CrossRef]
14. Kwon, H.-S.; Ryu, M.H.; Carlsten, C. Ultrafine particles: Unique physicochemical properties relevant to health and disease. *Exp. Mol. Med.* **2020**, *52*, 318–328. [CrossRef]
15. Molnár, A.; Imre, K.; Ferenczi, Z.; Kiss, G.; Gelencsér, A. Aerosol hygroscopicity: Hygroscopic growth proxy based on visibility for low-cost PM monitoring. *Atmos. Res.* **2020**, *236*, 104815. [CrossRef]
16. Liang, Z.; Chu, Y.; Gen, M.; Chan, C.K. Single-particle Raman spectroscopy for studying physical and chemical processes of atmospheric particles. *Atmos. Chem. Phys.* **2022**, *22*, 3017–3044. [CrossRef]
17. Doughty, D.C.; Hill, S.C. Raman spectra of atmospheric aerosol particles: Clusters and time-series for a 22.5 hr sampling period. *J. Quant. Spectrosc. Radiat. Transf.* **2020**, *248*, 106907. [CrossRef]
18. Estefany, C.; Sun, Z.; Hong, Z.; Du, J. Raman spectroscopy for profiling physical and chemical properties of atmospheric aerosol particles: A review. *Ecotoxicol. Environ. Saf.* **2023**, *249*, 114405. [CrossRef]
19. Andreae, M.O.; Charlson, R.J.; Bruynseels, F.; Storms, H.; Van Grieken, R.; Maenhaut, W. Internal Mixture of Sea Salt, Silicates, and Excess Sulfate in Marine Aerosols. *Science* **1986**, *232*, 1620–1623. [CrossRef]
20. Morillas, H.; Maguregui, M.; García-Florentino, C.; Marcaida, I.; Madariaga, J.M. Study of particulate matter from Primary/Secondary Marine Aerosol and anthropogenic sources collected by a self-made passive sampler for the evaluation of the dry deposition impact on built heritage. *Sci. Total Environ.* **2016**, *550*, 285–296. [CrossRef]
21. Li, D.; Yue, W.; Gong, T.; Gao, P.; Zhang, T.; Luo, Y.; Wang, C. A comprehensive SERS, SEM and EDX study of individual atmospheric PM2.5 particles in Chengdu, China. *Sci. Total Environ.* **2023**, *883*, 163668. [CrossRef]
22. Sobanska, S.; Falgayrac, G.; Rimetz-Planchon, J.; Perdrix, E.; Brémard, C.; Barbillat, J. Resolving the internal structure of individual atmospheric aerosol particle by the combination of Atomic Force Microscopy, ESEM–EDX, Raman and ToF–SIMS imaging. *Microchem. J.* **2014**, *114*, 89–98. [CrossRef]
23. Godoi, R.H.M.; Potgieter-Vermaak, S.; De Hoog, J.; Kaegi, R.; Van Grieken, R. Substrate selection for optimum qualitative and quantitative single atmospheric particles analysis using nano-manipulation, sequential thin-window electron probe X-ray microanalysis and micro-Raman spectrometry. *Spectrochim. Acta Part B At. Spectrosc.* **2006**, *61*, 375–388. [CrossRef]
24. González, L.T.; Longoria-Rodríguez, F.E.; Sánchez-Domínguez, M.; Leyva-Porras, C.; Acuña-Askar, K.; Kharissov, B.I.; Arizpe-Zapata, A.; Alfaro-Barbosa, J.M. Seasonal variation and chemical composition of particulate matter: A study by XPS, ICP-AES and sequential microanalysis using Raman with SEM/EDS. *J. Environ. Sci.* **2018**, *74*, 32–49. [CrossRef]
25. Stefaniak, E.A.; Buczynska, A.; Novakovic, V.; Kuduk, R.; Grieken, R.V. Determination of chemical composition of individual airborne particles by SEM/EDX and micro-Raman spectrometry: A review. *J. Phys. Conf. Ser.* **2009**, *162*, 012019. [CrossRef]
26. González, L.T.; Pérez-Rodríguez, M.; Rodríguez, F.E.L.; Mancilla, Y.; Acuña-Askar, K.; Campos, A.; Peña González, L.A.; Silva Vidaurri, L.G.; Zapata, A.A.; Nucamendi, A.; et al. Insights from the combined bulk chemical and surface characterization of airborne PM10 on source contributions and health risk: The case of three Mexican cities. *Air Qual. Atmos. Health* **2023**, *16*, 1455–1477. [CrossRef]
27. Longoria-Rodríguez, F.E.; González, L.T.; Mancilla, Y.; Acuña-Askar, K.; Arizpe-Zapata, J.A.; González, J.; Kharissova, O.V.; Mendoza, A. Sequential SEM-EDS, PLM, and MRS Microanalysis of Individual Atmospheric Particles: A Useful Tool for Assigning Emission Sources. *Toxics* **2021**, *9*, 37. [CrossRef]
28. Lafuente, B.; Downs, R.T.; Yang, H.; Stone, N. The power of databases: The RRUFF project. In *Highlights in Mineralogical Crystallography*; Armbruster, T., Danisi, R.M., Eds.; De Gruyter: Berlin, Germany, 2015; pp. 1–30. ISBN 978-3-11-041704-3.

29. Yadav, H.; Mehta, M.; Jain, S.; Singh, S.; Bhandari, S.; Nihalani, S. Trend Analysis for Different Types of Aerosols in Conjugation with Temperatures for the Indian Region During the Post-monsoon Season (1980–2019). *Aerosol Sci. Eng.* **2024**, *8*, 13–19. [CrossRef]
30. Allen, H.M.; Draper, D.C.; Ayres, B.R.; Ault, A.; Bondy, A.; Takahama, S.; Modini, R.L.; Baumann, K.; Edgerton, E.; Knote, C.; et al. Influence of crustal dust and sea spray supermicron particle concentrations and acidity on inorganic NO_3^- aerosol during the 2013 Southern Oxidant and Aerosol Study. *Atmos. Chem. Phys.* **2015**, *15*, 10669–10685. [CrossRef]
31. Wang, M.; Zheng, N.; Zhao, D.; Shang, J.; Zhu, T. Using Micro-Raman Spectroscopy to Investigate Chemical Composition, Mixing States, and Heterogeneous Reactions of Individual Atmospheric Particles. *Environ. Sci. Technol.* **2021**, *55*, 10243–10254. [CrossRef]
32. Morillas, H.; Marcaida, I.; García-Florentino, C.; Maguregui, M.; Arana, G.; Madariaga, J.M. Micro-Raman and SEM-EDS analyses to evaluate the nature of salt clusters present in secondary marine aerosol. *Sci. Total Environ.* **2018**, *615*, 691–697. [CrossRef]
33. Xu, P.; Xu, J.; He, M.; Song, L.; Chen, D.; Guo, G.; Dai, H. Morphology and chemical characteristics of micro- and Nano-particles in the haze in Beijing studied by XPS and TEM/EDX. *Sci. Total Environ.* **2016**, *565*, 827–832. [CrossRef]
34. Schwan, J.; Ulrich, S.; Batori, V.; Ehrhardt, H.; Silva, S.R.P. Raman spectroscopy on amorphous carbon films. *J. Appl. Phys.* **1996**, *80*, 440–447. [CrossRef]
35. Chen, Y.; Shah, N.; Huggins, F.E.; Huffman, G.P.; Linak, W.P.; Miller, C.A. Investigation of primary fine particulate matter from coal combustion by computer-controlled scanning electron microscopy. *Fuel Process. Technol.* **2004**, *85*, 743–761. [CrossRef]
36. Patiño, D.; Pérez-Orozco, R.; Porteiro, J.; Lapuerta, M. Characterization of biomass PM emissions using thermophoretic sampling: Composition and morphological description of the carbonaceous residues. *J. Aerosol Sci.* **2019**, *127*, 49–62. [CrossRef]
37. Wang, M.; Hu, T.; Wu, F.; Duan, J.; Song, Y.; Zhu, Y.; Xue, C.; Zhang, N.; Zhang, D. Characterization of PM2.5 Carbonaceous Particles with a High-Efficiency SEM: A Case Study at a Suburban Area of Xi'an. *Aerosol Sci. Eng.* **2021**, *5*, 70–80. [CrossRef]
38. Guedes, A.; Ribeiro, H.; Fernández-González, M.; Aira, M.J.; Abreu, I. Pollen Raman spectra database: Application to the identification of airborne pollen. *Talanta* **2014**, *119*, 473–478. [CrossRef]
39. Schulte, F.; Lingott, J.; Panne, U.; Kneipp, J. Chemical Characterization and Classification of Pollen. *Anal. Chem.* **2008**, *80*, 9551–9556. [CrossRef]
40. Zimmermann, B. Characterization of Pollen by Vibrational Spectroscopy. *Appl. Spectrosc.* **2010**, *64*, 1364–1373. [CrossRef]
41. Ahlrichs, R.; Ochsenfeld, C. Theoretical Treatment of Sodium Chloride Clusters. *Ber. Bunsenges. Phys. Chem.* **1992**, *96*, 1287–1294. [CrossRef]
42. Mazza, T.; Barborini, E.; Piseri, P.; Milani, P.; Cattaneo, D.; Li Bassi, A.; Bottani, C.E.; Ducati, C. Raman spectroscopy characterization of TiO_2 rutile nanocrystals. *Phys. Rev. B* **2007**, *75*, 045416. [CrossRef]
43. Morillas, H.; Marcaida, I.; Maguregui, M.; Upasen, S.; Gallego-Cartagena, E.; Madariaga, J.M. Identification of metals and metalloids as hazardous elements in PM2.5 and PM10 collected in a coastal environment affected by diffuse contamination. *J. Clean. Prod.* **2019**, *226*, 369–378. [CrossRef]
44. Curci, G.; Ferrero, L.; Tuccella, P.; Barnaba, F.; Angelini, F.; Bolzacchini, E.; Carbone, C.; Denier Van Der Gon, H.A.C.; Facchini, M.C.; Gobbi, G.P.; et al. How much is particulate matter near the ground influenced by upper-level processes within and above the PBL? A summertime case study in Milan (Italy) evidences the distinctive role of nitrate. *Atmos. Chem. Phys.* **2015**, *15*, 2629–2649. [CrossRef]
45. Wu, L.; Eom, H.-J.; Yoo, H.; Gupta, D.; Cho, H.-R.; Fu, P.; Ro, C.-U. Chemical composition-dependent hygroscopic behavior of individual ambient aerosol particles collected at a coastal site. *Atmos. Chem. Phys.* **2023**, *23*, 12571–12588. [CrossRef]
46. Jacobson, M.Z. *Fundamentals of Atmospheric Modeling*, 2nd ed.; Cambridge University Press: Cambridge, UK, 2005; ISBN 978-0-511-11115-0.
47. Ansari, A. Prediction of multicomponent inorganic atmospheric aerosol behavior. *Atmos. Environ.* **1999**, *33*, 745–757. [CrossRef]